Structure and Function of Prokaryotic Glutamate Transporters from *Escherichia coli and Pyrococcus horikoshii*†

Stefan Raunser,[‡,§] Matthias Appel,[‡,§] Constanta Ganea,[||,⊥] Ulrike Geldmacher-Kaufer,[‡] Klaus Fendler,[||] and Werner Kühlbrandt*[,‡]

Departments of Structural Biology and Biophysical Chemistry, Max-Planck-Institute of Biophysics, Max-von-Laue-Strasse 3, 60438 Frankfurt am Main, Germany, and Department of Biophysics, C. Davila Medical University, Eroii Sanitari Blvd. 8, 76241 Bucharest, Romania

Received May 20, 2006; Revised Manuscript Received August 21, 2006

ABSTRACT: The glutamate transporters $GltP_{Ec}$ from *Escherichia coli* and $GltP_{Ph}$ from *Pyrococcus horikoshii* were overexpressed in *E. coli* and purified to homogeneity with a yield of 1−2 mg/L of culture. Single-particle analysis and electron microscopy indicate that $GltP_{Ph}$ is a trimer in detergent solution. Electron microscopy of negatively stained $GltP_{Ph}$ two-dimensional crystals shows that the transporter is a trimer also in the membrane. Gel filtration of $GltP_{Ec}$ indicates a reversible equilibrium of two oligomeric states in detergent solution that we identified as a trimer and hexamer by blue-native gel electrophoresis and cross-linking. The purified transporters were fully active upon reconstitution into liposomes, as demonstrated by the uptake of radioactively labeled L-aspartate or L-glutamate. L-Aspartate/L-glutamate transport of $GltP_{Ec}$ involves the cotransport of protons and depends only on pH, whereas $GltP_{Ph}$ catalyzes L-glutamate transport with a cotransport of H^+ or Na^+. L-Glutamate induces a fast transient current in $GltP_{Ph}$ proteoliposomes coupled to a solid supported membrane (SSM). We show that the electric signal depends on the concentration of Na^+ or H^+ outside the proteoliposomes and that $GltP_{Ph}$ does not require K^+ inside the proteoliposomes. In addition, the electrical currents are inhibited by TBOA and HIP-B. The half-saturation concentration for activation of $GltP_{Ph}$ glutamate transport ($K_{0.5}^{glut}$) is 194 μM.

Glutamate is the major excitatory neurotransmitter in the vertebrate central nervous system and is probably involved in most aspects of normal brain function, including cognition, memory, and learning (*1*). The concentration of glutamate in the synaptic cleft is regulated by secondary transporters, of which five have so far been identified and cloned (*2*−*6*). One glutamate is taken up together with three Na^+ ions and one H^+ in exchange for one K^+ (*7*−*9*). In bacteria, glutamate serves as a source for carbon and nitrogen under nitrogen-limiting conditions and is taken up by a cotransport of protons and/or sodium. However, wild-type strains of *Escherichia coli* cannot grow with glutamate as the sole source of carbon and nitrogen. This inability seems to result from their low activity for glutamate uptake, and in fact, mutants that have acquired higher glutamate uptake activity can grow on glutamate (*10*).

In *E. coli*, three L-glutamate transport systems have been identified: (i) a binding protein-dependent, glutamate/aspartate transport system, (ii) a sodium-dependent glutamate-specific system (GltS), and (iii) a proton symport system for glutamate and aspartate ($GltP_{Ec}$) (*11*−*15*). $GltP_{Ec}$ catalyzes an electrogenic symport of L-glutamate with at least two protons (*16*). Besides the glutamate transporters of *E. coli*, only three more bacterial glutamate transport systems have been functionally characterized (*Bacillus caldotenax*, *Bacillus subtilis*, and *Bacillus stearothermophilus*) (*16*). An exact determination of the uptake stoichiometry of bacterial glutamate transporters has not been reported since their functional expression in *Xenopus laevis* oocytes might be impossible.

Prokaryotic and eukaryotic glutamate transporters are members of the glutamate transporter family that also comprises neutral amino acid, amino acid, and dicarboxylic acid transporters. They possess major amino acid sequence relationships and differ in their structure significantly from other secondary transporters. For instance, the polypeptide sequences of *E. coli* glutamate transporter $GltP_{Ec}$ and *Pyrococcus horikoshii* glutamate transporter $GltP_{Ph}$ are 33% identical and 55% homologous. Both are highly homologous (44 and 48%, respectively) to GLT-1, the glial glutamate transporter in mammals. The region between helix 6 and helix 8 that is crucial for binding and transport of substrate and ions is particularly highly conserved.

Recently, the first high-resolution structure of a glutamate transporter homologue from *P. horikoshii* ($GltP_{Ph}$) was reported (*17*). However, a transport activity of the reconstituted transporter could not be measured. The $GltP_{Ph}$ crystal

† This work was partly supported by a Ph.D. fellowship of "Studienstiftung des deutschen Volkes".

* To whom correspondence should be addressed: Department of Structural Biology, Max-Planck-Institute of Biophysics, Max-von-Laue-Str. 3, 60438 Frankfurt am Main, Germany. E-mail: Werner.Kuehlbrandt@mpibp-frankfurt.mpg.de. Phone: +49-69-6303-3000. Fax: +49-69-6303-3002.

‡ Department of Structural Biology, Max-Planck-Institute of Biophysics.

§ These authors contributed equally to this work.

|| Department of Biophysical Chemistry, Max-Planck-Institute of Biophysics.

⊥ C. Davila Medical University.

10.1021/bi061008+ CCC: $33.50
Published on Web 10/03/2006

structure indicated that it is a trimer. Trimeric assemblies were also reported for the glutamate transporter from *B. caldotenax* and *B. stearothermophilus* (*18*) and may also be conserved in human glutamate transporters (*19*, *20*).

Here we report the overexpression, purification, and functional and structural characterization of *E. coli* glutamate transporter $GltP_{Ec}$ and *P. horikoshii* glutamate transporter $GltP_{Ph}$. Glutamate transport kinetics of $GltP_{Ph}$ were measured using the solid-supported membrane (SSM) technique. Two-dimensional (2D) crystals of the $GltP_{Ph}$ transporter indicate that it is a trimer in the membrane.

MATERIALS AND METHODS

Cloning and Cell Culture. Genomic DNA of *P. horikoshii* was obtained from ATCC (catalog no. 700860D). The locus PH1295, encoding the hypothetical proton/sodium glutamate symport protein ($GltP_{Ph}$), was amplified by polymerase chain reaction using recombinant Taq and Tgo polymerase. The $GltP_{Ph}$ gene was inserted into the pET-28a plasmid (Novagen) with a His_6 tag fused to the N- and C-termini. The gene encoding the *E. coli* proton/sodium symport protein ($GltP_{Ec}$) was amplified by PCR using the *E. coli* BL21(DE3) strain as a template, with forward and reverse primers designed according to the published DNA sequence of the protein (*21*, *22*). The gene was cloned in a pET 20 vector with a His_6 tag fused to the C-terminus. The insert was sequenced (MWG Biotech) and found to be the same as the published base sequence of the gltP gene (*21*) except for a point mutation at position 895 which results in a Val298Ala mutation. Both transporters were expressed in the C-43 strain of *E. coli* (Avidis), following standard molecular biology protocols (*23*). In the case of $GltP_{Ec}$, 12 L of 2× YT medium was inoculated at 30 °C with an overnight culture, followed by induction with 0.6 mM IPTG at an OD_{600} of 0.9. Cells were harvested 2−3 h after induction at an OD_{600} of 1.6−1.9. In the case of $GltP_{Ph}$, 12 L of TB medium was inoculated with an overnight culture, followed by induction with 1 mM IPTG at an OD_{600} of 1. Cells, growing at 30 °C, were harvested 12 h after induction.

Protein Purification. Cells were resuspended in homogenization buffer [10 mM Tris-HCl (pH 7.4), 10% glycerol, 150 mM KCl, 1 mM EDTA, and 1 mM PMSF] and broken by two passages through a cell disrupter (Constant Systems) operated at 1.5 kbar. Unbroken cells were removed at 6500*g* for 15 min followed by an ultracentrifugation at 150000*g* for 90 min at 4 °C to collect the membrane fraction. Membranes were resuspended in homogenization buffer at a protein concentration of 15 mg/mL and stored at −80 °C; 12 mL of the membrane suspension (15 mg/mL) was solubilized in 24 mL of buffer A [150 mM Tris-HCl (pH 7.5), 1.5% dodecyl maltoside (DDM) or decyl maltoside (DM), 30% glycerol, and 10 mM imidazole] for 1 h at 4 °C on a shaker. Undissolved material was removed by centrifugation at 100000*g* for 30 min at 4 °C.

Solubilized protein was mixed with 2 mL of Ni^{2+}−NTA agarose beads (QIAGEN), equilibrated in buffer B [5 mM imidazole, 500 mM NaCl, 20 mM Tris-HCl (pH 7.9), and 0.1% DDM or 0.4% DM], incubated for 1 h at 4 °C under continuous shaking, and, subsequently, poured into a column. The column was washed with 10 column volumes of buffer B and 20 column volumes of buffer C [30 mM imidazole, 500 mM NaCl, 20 mM Tris-HCl (pH 7.9), 0.1% DDM or 0.4% DM, and 10% glycerol]. The protein was eluted in buffer D [150 mM imidazole, 300 mM NaCl, 0.1% DDM or 0.2% DM, 10% glycerol, and 20 mM Tris-HCl (pH 7.9)]. Analytical gel filtration was performed at 4 °C on a SMART system (Amersham) using a Superose-6 column at a flow rate of 40 μL/min.

Reconstitution of Purified $GltP_{Ec}$ and $GltP_{Ph}$ in Liposomes and Transport Assays. Liposomes were prepared as described previously (*19*). *E. coli* polar lipids (Avanti) were used instead of the asolectin/brain polar lipid mixture; 50 mg of lipids was suspended in 1 mL of dialysis buffer [120 mM KP_i (pH 7.4), 1% glycerol, 5 mM Tris-SO_4 (pH 7.4), 0.5 mM Na-EDTA, and 1 mM $MgSO_4$]. Reconstitution and uptake of [^{3}H]-L-aspartate (Amersham) or [^{3}H]-L-glutamate (Amersham) were assessed as described previously (*19*). For each time point, 20 μL of proteoliposomes was added to 360 μL of influx solution containing 150 mM NaCl or 150 mM choline chloride, 10 mM KP_i (pH 7.4) or 10 mM KAc (pH 4.7), 1 μCi of [^{3}H]-L-aspartate (29 Ci/mmol) or [^{3}H]-L-glutamate (42 Ci/mmol), and 2.5 μM valinomycin. Nitrocellulose filters with a pore size of 0.45 μm were used.

Transport Activity Assay on a Solid-Supported Membrane (SSM). The SSM, an octadecyl mercaptane monolayer covered with a diphytanoylphosphatidylcholine monolayer on a gold electrode, was mounted in a flow-through cuvette. Proteoliposomes were thawed, sonicated, and allowed to adsorb to the SSM. A rapid solution exchange in the cuvette allowed the generation of substrate concentration jumps at the SSM. The solution exchange protocol consisted of five steps each 1 s in duration: (1) resting solution, (2) nonactivating solution, (3) activating solution (concentration jump), (4) nonactivating solution, and (5) resting solution. The resting solutions (1 and 5) contained 150 mM K^+ to maintain a high K^+ concentration in the liposomes. Activating and nonactivating solutions contained 150 mM Na^+ and no K^+, respectively, to establish a Na^+ and K^+ gradient across the liposomal membrane. In addition, the activating solution contained 1 mM L-glutamate. The current generated by the glutamate transporter in response to a glutamate concentration jump was recorded at the gold electrode via capacitive coupling. For details, see refs *24* and *25*.

Activating and nonactivating solutions contained 30 mM Hepes (pH 7.4) or 30 mM acetate (pH 4.7), 2 mM $MgCl_2$, 0.3 mM $CaCl_2$, 0.1 mM dithiothreitol (DTT, 99.5%, Roth, Karlsruhe, Germany), salts (150 mM NaCl, 150 mM KCl, or 150 mM choline chloride), and L-glutamic acid at various concentrations. The protein concentration in the proteoliposome suspension was ∼0.5 mg/mL. The lipid film-forming solution contained diphytanoylphosphatidylcholine (PC, synthetic, Avanti Polar Lipids Inc., Pelham, AL) and octadecylamine (60:1, w/w, 98%, Riedel-de-Haen AG, Seelze-Hannover, Germany) prepared at a concentration of 1.5% in *n*-decane (*26*). A 1 mM octadecylmercaptan (C_{18}-mercaptan, Aldrich, Steinheim, Germany) solution in ethanol was used for the incubation of the gold electrodes.

Cross-Linking of Membrane Proteins. Prior to cross-linking experiments, the protein was dialyzed against buffer A [25 mM KP_i (pH 7.4), 300 mM NaCl, 10% glycerol, and 0.1% DDM]. To 30 μg of protein were added different cross-linkers. Disuccinimidyl suberate (DSS) (Sigma) was solubilized in DMSO (dimethyl sulfoxide) and added to a final

concentration of 1, 10, or 50 mM. For control, DMSO was added alone. Glutaraldehyde (Agar Scientific, Stansted, U.K.) was added to a final concentration of 2.5 or 5 mM. After the mixtures were incubated for 30 min at room temperature, the reactions were quenched by addition of 200 mM Tris-HCl (pH 7.4). The cross-linked samples were then analyzed on a Coomassie-stained SDS−PAA gel.

Protein Concentration and Gel Electrophoresis. The membrane protein concentration was determined by the Bradford method (*27*) with bovine serum albumin as a standard. For SDS−PAGE, proteins were separated on a 10% (w/v) polyacrylamide gel. After electrophoresis, the proteins were stained with Coomassie Brilliant Blue. For blue-native gel electrophoresis (*28*, *29*), linear 6 to 16.5% (w/v) polyacrylamide gradient separation gels were used with a 5% stacking gel overlay. Gel dimensions were 180 mm × 160 mm × 1 mm. Protein samples were supplemented with a 10-fold concentrated loading dye [5% Coomassie Brilliant Blue, 500 mM 6-amino-*n*-caproic acid, and 100 mM Bis-Tris (pH 7.0)].

Single-Particle Analysis. Single-particle analysis was conducted as described previously (*19*). Protein was diluted to a final concentration of 0.01 mg/mL and applied onto glow-discharged 400-mesh copper grids coated with a thin carbon film. The specimens were negatively stained with 1.5% uranyl acetate. Electron micrographs were recorded under low-dose conditions on a Philips CM120 electron microscope at an accelerating voltage of 100 kV and calibrated magnification of 58600×; the defocus of the images ranged from 1.0 to 2 μm. Micrographs selected for image processing were digitized using a SCAI scanner (ZEISS) with a final pixel size of 7 μm.

Single particles were selected manually using WEB (*30*), and the images were processed using SPIDER (*30*). The selected particles were windowed into 80 × 80 pixel boxes and normalized (*31*). The images were centered, and a first reference was obtained by a reference-free alignment (*32*). All the particles were then aligned to this new reference using simultaneous translational/rotational algorithms based on cross correlations of two-dimensional Radon transforms (*33*, *34*). The aligned particles were classified using pattern recognition by a neuronal network algorithm (*35*) of XMIPP (*36*) using a field of 7 × 7 nodes. Several nodes were selected and used as references in multireference alignments. The aligned particles were assigned to the reference for which they exhibited the highest cross-correlation coefficient. Neuronal network analyses and multireference alignments were done several times until the particles in a class converged to a homogeneous shape.

Two-Dimensional Crystallization, Electron Microscopy, and Image Processing. Crystallization was performed by detergent dialysis. Solubilized protein [~1 mg/mL protein in 0.1% (w/v) DDM] was added to detergent-solubilized *E. coli* polar lipids (Avanti) in DM at lipid:protein ratios of 0.25−1.0 (w/w). Samples (100 μL) were first incubated for 1 day at 22 °C and were then dialyzed for 7 days against 20 mM Tris-HCl (pH 7.5), 100 mM NaCl, 10% glycerol, and 3 mM NaN_3 at 30 °C.

Crystals were negatively stained with 1.5% (w/v) uranyl acetate. Electron micrographs were recorded under low-dose conditions on a Philips CM12 microscope at a magnification of 45000×.

Selected image areas of 4000 × 4000 pixels were digitized on a SCAI scanner (Zeiss) with a pixel size of 7 μm. Images were processed using the MRC image processing programs (*37*, *38*).

RESULTS

Protein Purification. Several detergents were tested for solubilization and purification, but only DDM or DM was efficient in keeping the protein stable, without aggregation or loss of activity as determined by electron microscopy and glutamate uptake measurements (data not shown). The proteins were purified in a single step by Ni^{2+}−NTA affinity chromatography. The isolated protein was pure as judged by Coomassie-stained SDS−PAGE (Figure 1A,B). Both $GltP_{Ph}$ and $GltP_{Ec}$ appeared as strong distinct bands at ~35 kDa. The apparent molecular mass of both proteins is different from their calculated molecular masses of 45 and 47 kDa, respectively, which is the case for many membrane proteins (*19*, *39*). We obtained typically 1−2 mg of pure protein from 1 L of culture. As determined by electron microscopy, $GltP_{Ec}$ was stable for ~1 week, whereas $GltP_{Ph}$ was stable for up to 4 weeks at 4 °C, without aggregation or proteolysis (data not shown).

When the detergent-solubilized, purified proteins were subjected to gel filtration chromatography (Figure 1C), a main peak (retention volume of 1.55 mL) with a smaller shoulder at a higher molecular mass (retention volume of 1.36 mL) was observed for $GltP_{Ec}$. $GltP_{Ph}$ eluted from the column as a single peak with a retention volume of 1.57 mL. The $GltP_{Ph}$ transporter also appeared to be monodisperse at higher protein concentrations (data not shown). The column was calibrated with soluble proteins with known Stokes radii. By these standards, the Stokes radius of $GltP_{Ph}$ was ~59 Å and that of $GltP_{Ec}$ ~60 Å for the main peak and ~76 Å for the shoulder.

$GltP_{Ec}$ Oligomeric States in a Detergent Solution. The gel filtration profile of $GltP_{Ec}$ was further investigated. We found that the height of the $GltP_{Ec}$ shoulder depended on the protein concentration, with more of the higher molecular mass appearing at higher protein concentrations (Figure 1D). Concentrating the transporter did not result in aggregates that would elute at the void volume. Dilution of samples with higher protein concentrations resulted in a shift to a lower molecular mass (Figure 2E). However, the shift from the higher to the lower molecular mass was slow and complete after only 1 day. This indicated a reversible equilibrium between at least two forms of $GltP_{Ec}$ that differed in size, which was shifted to a higher molecular mass at higher protein concentrations. Furthermore, the gel filtration profile depended on the type of detergent used (Figure 1E). The gel filtration profile did not change significantly after storage for 1 week at 4 °C (data not shown), indicating that the higher oligomeric forms of $GltP_{Ec}$ were stable in solution.

When the purified protein was solubilized in DDM, the shoulder at the higher molecular mass became more prominent compared to that of $GltP_{Ec}$ solubilized in DM. $GltP_{Ec}$ solubilized even at low protein concentrations in FOS-choline 12 or $C_{12}E_9$ resulted in a shift toward the higher molecular mass.

Since we found two forms of $GltP_{Ec}$ of different sizes that could correspond to two different oligomeric states, we used

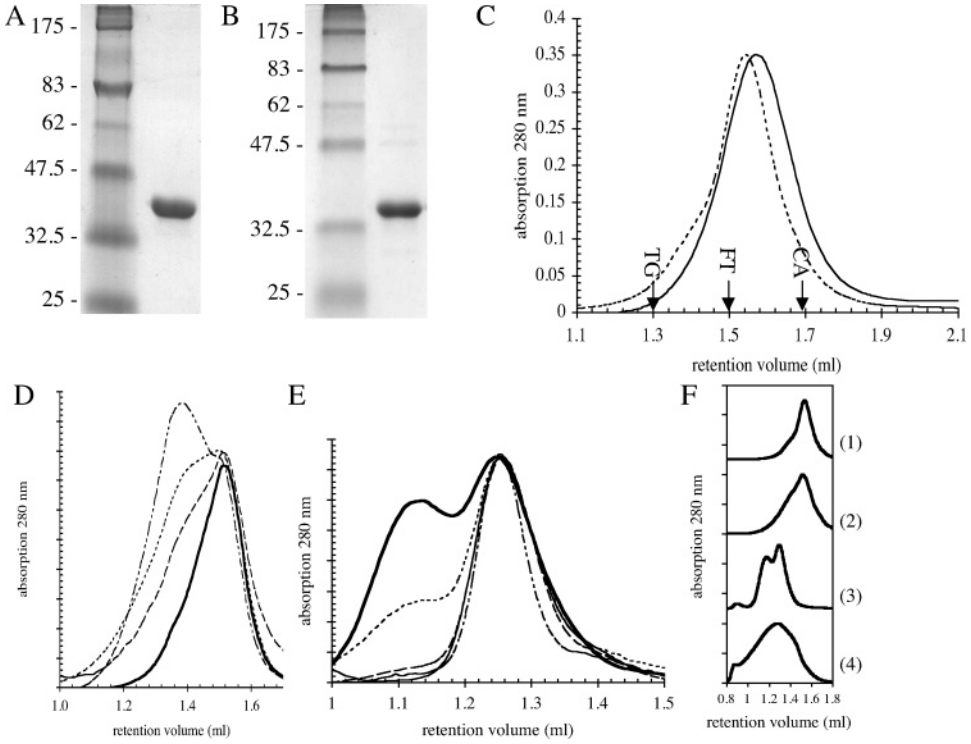

FIGURE 1: SDS−PAGE of purified $GltP_{Ec}$ and $GltP_{Ph}$. $GltP_{Ec}$ (A) and $GltP_{Ph}$ (B) were eluted from a Ni−NTA column, analyzed by SDS−PAGE, and stained with Coomassie Brilliant Blue. (C) Superose-6 gel filtration of $GltP_{Ec}$ and $GltP_{Ph}$ in DM. The proteins solubilized in DM were eluted from a Ni−NTA column and further purified with a Superose-6 column on a SMART system at 4 °C. The absorption was normalized to the highest peak. Retention volumes of standard proteins of known Stokes radius are indicated: TG, thyroglobulin (86 Å); FT, ferritin (63 Å); and CA, catalase (52 Å). (D) Analytical gel filtration of $GltP_{Ec}$ on a Superose-6 column. Different concentrations of purified $GltP_{Ec}$ in DDM were analyzed: 6 (− - - −), 2 (- - -), 0.2 (− − −), and 0.02 mg/mL (—). The absorption was normalized to the main peak. (E) Analytical gel filtration profile of 0.2 mg/mL $GltP_{Ec}$ solubilized in FOS-choline12 (thick solid line). Eluted protein at a retention volume of 1.12 mL from the first run was rerun after 30 min (- - -) and after 1 day (− - - −). This was repeated for eluted protein at a retention volume of 1.25 mL after 30 min (− − −) and after 1 day (—). The protein was diluted ∼5−6-fold after the first run. The absorption was normalized to the main peak. (F) Purified $GltP_{Ec}$ solubilized in different detergents was analyzed on a Superose-6 column at a concentration of 0.2 mg/mL: (1) DM, (2) DDM, (3) FOS-choline 12, and (4) $C_{12}E_9$. The absorption was normalized to the highest peak.

blue-native gel electrophoresis and cross-linking to determine the size of the observed $GltP_{Ec}$ oligomers.

Blue-native gel electrophoresis of $GltP_{Ec}$ indicated a band of ∼220 and ∼440 kDa using soluble protein markers as standards (Figure 2A, lane 1). Using a factor of 1.8 to compensate for the larger apparent mass of membrane proteins on blue-native gels (*40*), the apparent molecular masses of the 440 and 220 kDa bands correspond roughly to a hexamer (280 kDa) and trimer (140 kDa), respectively. Titration with SDS resulted in partial dissociation of the oligomeric assembly, evident in a ladderlike pattern of three bands (∼200, ∼130, and ∼60 kDa) (Figure 2A, lane 2). The reduction in apparent molecular mass can be explained by the negative charge of SDS and by partial denaturation that makes proteins run faster in the gel. This clearly identified the 220 kDa band as the $GltP_{Ec}$ trimer.

Cross-linking of the purified $GltP_{Ec}$ complex resulted in only trimers as the biggest oligomers when cross-linkers with short spacer arms (glutaraldehyde, 7.2 Å) were used (Figure 2B, lanes 5 and 6). Treatment with cross-linkers with longer spacer arms (DSS, 11.4 Å) resulted in hexamers as the strongest band at higher molecular masses (Figure 2B, lanes 2−4).

$GltP_{Ph}$ Forms Trimers in the Membrane and in Detergent Solution. A $GltP_{Ph}$ trimer was found in detergent solution using single-particle analysis and electron microscopy; 2588 particles were selected from six electron micrographs (Figure 3) and subjected to several steps of alignment and classification. $GltP_{Ph}$ particles appeared to be homogeneous, and all particles aligned to a single class (Figure 3 inset) that exhibited three clear densities arranged in a triangle, with an edge length of ∼90 Å.

2D crystallization trials were carried out for both transporters. Both proteins could be easily reconstituted into liposomes at high protein density over a wide pH range as judged by freeze-fracture and electron microscopy (data not shown). $GltP_{Ph}$ formed crystalline sheets that typically grew out of tightly clustered proteoliposomes and tended to form multilayered stacks. An optimal LPR for crystallization was found at ∼0.7 (w/v) at pH 7.5. The crystals exhibited a hexagonal lattice (Figure 4A,B) and had 3-fold symmetry (*P*3) as indicated by ALLSPACE (*41*). A projection map at 25 Å was calculated with *P*3 symmetry applied (Figure 4C). The unit cell of the 2D crystals was as follows: $a = b = 95$ Å and $\gamma = 120°$. Calculated from the projection map, the dimensions of a GltP monomer were as follows: ∼31 Å × ∼46 Å. The diameter of the GltP trimer was ∼90 Å.

Reconstituted $GltP_{Ec}$ and $GltP_{Ph}$ Exhibit Highly Specific Aspartate/Glutamate Uptake. To prove the full activity of both GltP transporters after recombinant expression and purification, they were reconstituted into preformed *E. coli*

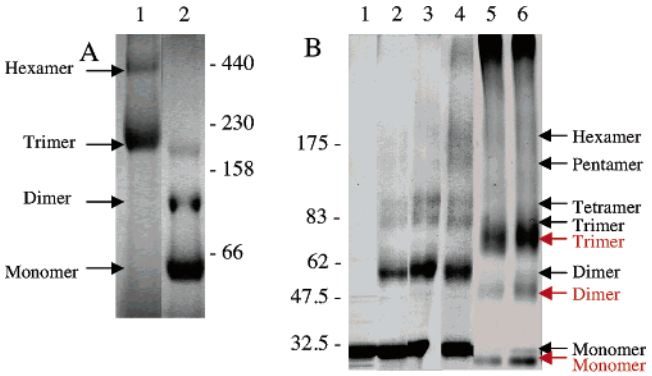

FIGURE 2: (A) Blue-native gel electrophoresis. Ten micrograms of purified $GltP_{Ec}$ transporter was mixed with sample buffer and separated on a blue-native gel (lanes 1 and 2). SDS (0.1%) was added to the sample prior to loading to achieve a partial dissociation of the $GltP_{Ec}$ complex (lane 2). (B) Cross-linking of $GltP_{Ec}$. Protein purified in DDM was incubated with DSS or glutaraldehyde in varying amounts for 30 min at room temperature, and the reaction was quenched with 200 mM Tris-HCl (pH 7.4). The cross-linked products were resolved on a 10% polyacrylamide−SDS gel and detected by Coomassie staining: lane 1, protein without cross-linker; lanes 2−4, 1, 10, and 50 mM DSS, respectively; and lanes 5 and 6, 2.5 and 5 mM glutaraldehyde, respectively. The bands corresponding to oligmers are denoted with red arrows for cross-linking with glutaraldehyde and with black arrows for cross-linking with DSS.

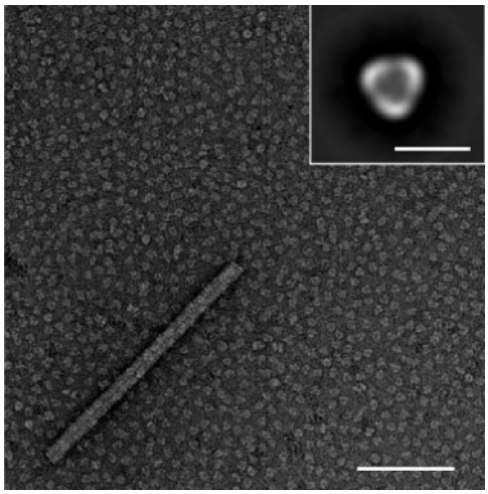

FIGURE 3: Single-particle analysis of $GltP_{Ph}$. Electron micrographs of negatively stained samples of $GltP_{Ph}$. The scale bar represents 100 nm; 2588 particles were selected. The inset shows a typical two-dimensional average of the proteins. The scale bar in the inset represents 10 nm.

polar lipid vesicles, and their specific activity was measured by uptake of [^{3}H]-L-aspartate or [^{3}H]-L-glutamate (Figure 5).

Studies with membrane vesicles from *E. coli* cells have shown that $GltP_{Ec}$ transports L-aspartate or L-glutamate across the membrane with the symport of at least two protons; a Na^+ gradient did not catalyze the transport at all (*16*).

Therefore, we assessed the time-dependent aspartate uptake of $GltP_{Ec}$ with a pH gradient as the driving force (Figure 5A).

The aspartate transport reached saturation after 400 s and was blocked by the nontransportable inhibitor (2*S*,4*R*)-4-methyl glutamate. After the addition of the ionophore monensin, which allows a Na^+/H^+ exchange across a membrane and breaks down a proton gradient, no aspartate uptake was recorded. The same result was obtained when

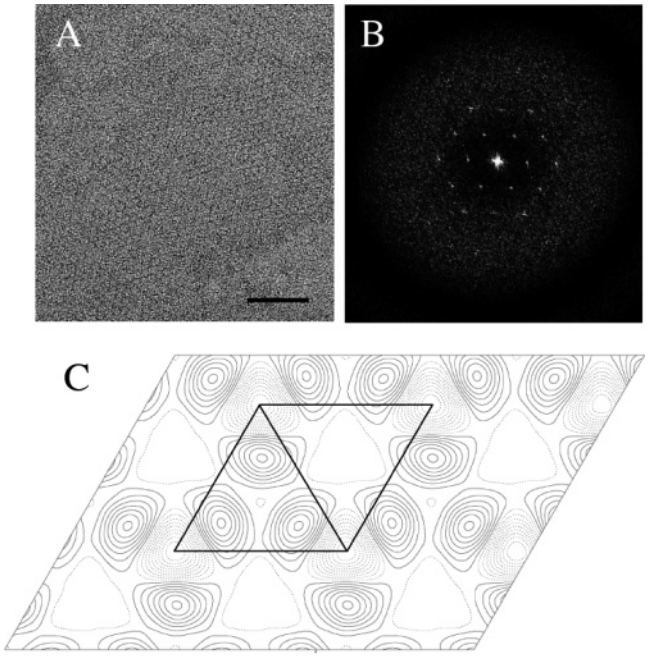

FIGURE 4: 2D crystallization of $GltP_{Ph}$. (A) 2D crystal lattice of a single membrane stained with 1.5% uranyl acetate and (B) its power spectrum. The scale bar is 100 nm. (C) Projection density map of negatively stained $GltP_{Ph}$ crystals at 25 Å resolution. *P*3 symmetry and an isotropic temperature factor (−200 Å^2) were applied.

no proton gradient was created on the membrane prior to uptake. A Na^+ gradient did not catalyze L-aspartate uptake (data not shown). Thus, the reconstituted $GltP_{Ec}$ transporter was fully functional and exhibited a highly specific aspartate transport that is driven by a proton gradient. The amount of transported aspartate depended on the proton concentration (Figure 5B). The lower the pH in the uptake buffer, the more aspartate was transported. Without a proton gradient (pH 7.4) or with an inverse gradient (pH >7.4), no transport was catalyzed.

For $GltP_{Ph}$, [^{3}H]-L-glutamate transport was assessed using either a Na^+ or a H^+ gradient at steady state (Figure 5D). Both Na^+ and H^+ catalyzed glutamate transport over the membrane, whereas no glutamate was transported without a gradient. As for $GltP_{Ec}$, the uptake was blocked by the nontransportable inhibitor (2*S*,4*R*)-4-methyl glutamate. We measured the rate of time-dependent glutamate uptake of $GltP_{Ph}$, applying a Na^+ gradient as the driving force (Figure 5C). The aspartate transport reached saturation after 250 s. Without a Na^+ gradient, no transport was observed.

We conclude that $GltP_{Ph}$ reconstituted in *E. coli* liposomes indeed functions as a specific glutamate transporter and is driven by a proton and/or Na^+ gradient.

Glutamate Induced Electrical Signals Generated by $GltP_{Ph}$ Proteoliposomes Coupled to a Solid-Supported Membrane (SSM). To investigate the transport kinetics of $GltP_{Ph}$ in more detail, we coupled proteoliposomes to a SSM. $GltP_{Ph}$ proteoliposomes and SSM form a capacity-coupled system that enables measurements of transient currents in response to rapid concentration jumps of $GltP_{Ph}$ substrates. Figure 6A (top trace) shows a typical current induced by a 2 mM concentration jump of L-glutamate in the presence of 150 mM NaCl. Na^+ was present 1 s before, during, and after the L-glutamate concentration jump so that sufficient time was given for Na^+ to bind to the enzyme before the signal was

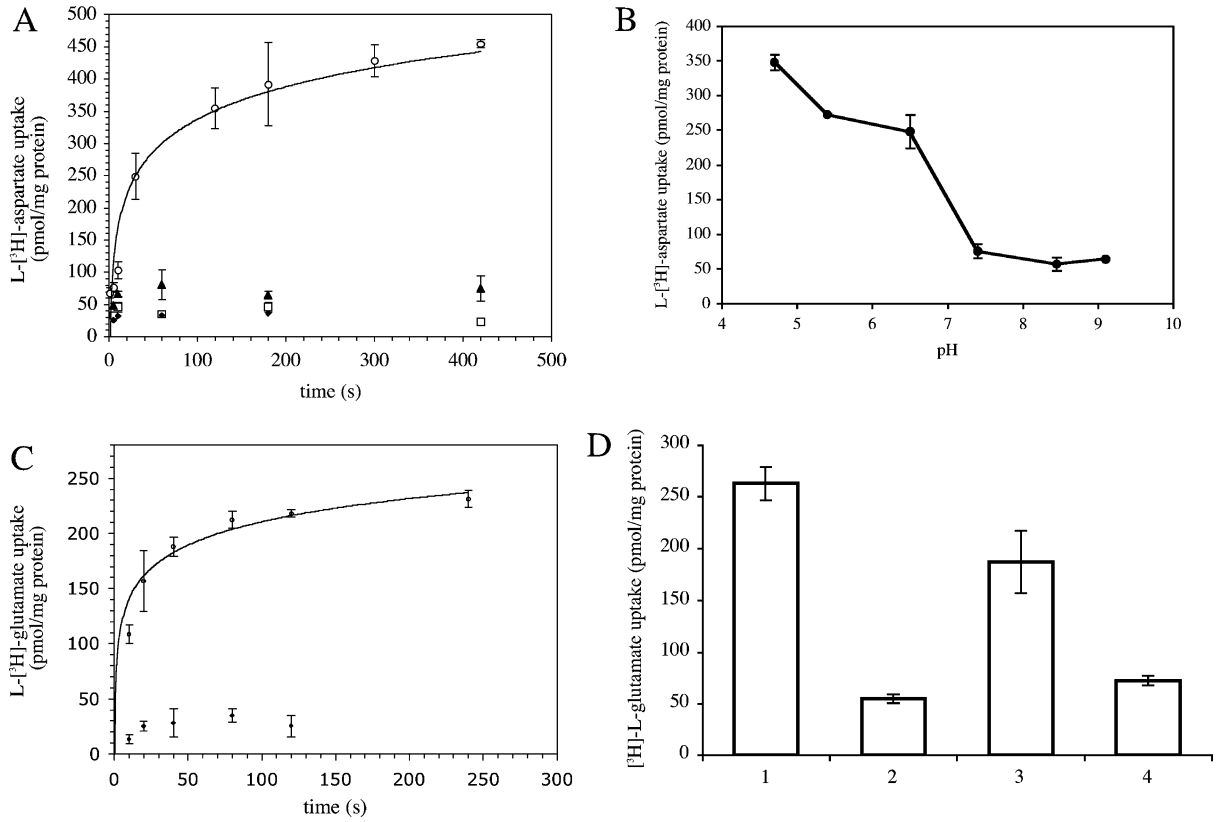

FIGURE 5: [^{3}H]-L-Aspartate transport of purified and reconstituted $GltP_{Ec}$ or $GltP_{Ph}$. (A) Purified $GltP_{Ec}$ was reconstituted in liposomes, and the transport of [^{3}H]-L-aspartate was dependent on time and measured using a pH gradient as the driving force: pH 4.7 outside and pH 7.4 inside (○). As a control, the experiments were performed with 250 μM (2*S*,4*R*)-4-methyl glutamate (SYM) as the inhibitor (□), with the Na^+/H^+ ionophore monensin (◆), or without a pH gradient [pH 7.4 outside and inside (▲)]. (B) [^{3}H]-L-Aspartate transport of purified and reconstituted $GltP_{Ec}$ at different pHs at steady state. The pH inside the liposomes for all measurements was pH 7.4. The uptake of [^{3}H]-L-aspartate was stopped after 10 min. (C) Purified $GltP_{Ph}$ was reconstituted in liposomes, and the time-dependent transport of [^{3}H]-L-glutamate was assessed using a Na^+ gradient to provide the driving force (150 mM NaCl in the influx solution). As a control, the experiments were performed without a Na^+ gradient (150 mM choline chloride) (◆). (D) [^{3}H]-L-Glutamate transport of purified and reconstituted $GltP_{Ph}$ was assessed, with a Na^+ gradient or a pH gradient providing the driving force (pH 4.7 outside and pH inside 7.4) at steady state. The uptake was stopped after 10 min: (1) 150 mM NaCl at pH 7.4, (2) 150 mM NaCl and 250 μM SYM as the inhibitor, (3) 150 mM choline chloride at pH 4.7, and (4) 150 mM choline chloride at pH 7.4.

recorded. At this stage of the preparation, the proteoliposomes were preloaded with 120 mM KP_i buffer. In addition, the SSM with adsorbed proteoliposomes was preincubated with 150 mM KCl in the resting solution before the experiment (30 min) and between experiments (~5 min), to ensure that the liposomes remain loaded with KCl during the experiment. Therefore, during the glutamate concentration jump, an inward Na^+ gradient and an outward K^+ gradient of 150 mM were present simultaneously.

The resulting electrical current was biphasic, characterized by a fast negative transient current followed by a slow positive phase. A biexponential fit yielded a time constant of ~8 ms for the decay of the negative component and for the positive component of ~70 ms. This indicates a rapid movement of a negative charge, followed by a slower movement of a positive charge into the liposomes (or of a positive charge followed by a negative charge in the opposite direction). A similar glutamate concentration jump (2 mM) performed with activating solutions containing either 150 mM KCl (Figure 6D, pH 7.4, bottom trace) or 150 mM choline chloride (Figure 6A, bottom trace) instead of NaCl yielded only a minor artifact.

Also, the requirement of K^+ inside the liposomes was tested. The proteoliposomes adsorbed to the SSM were incubated in K^+-free solution containing 150 mM NaCl in the presence of the alkali metal/H^+ exchanging ionophore nigericin (10 μM) for 30 min and then measured in K^+-free solutions, omitting the K^+-containing resting solution. Alternatively, proteoliposomes were prepared in K^+-free 120 mM NaP_i buffer and measured in a 150 mM NaCl-containing solution. No difference was observed with or without K^+ (data not shown). This demonstrated that neither an outward K^+ gradient nor indeed any K^+ ions at all are required for the observed transient charge displacement. Although no Na^+ gradient was applied in these experiments, we measured a transient charge displacement. This proves that Na^+ but no Na^+ gradient was necessary for pre steady-state glutamate uptake.

In many cases, Na^+-coupled transporters can use protons as an alternative substrate. Therefore, measurements were performed at neutral pH (7.4) and at acidic pH (4.7). This comparison is shown in Figure 6D. While at pH 7.4 in the absence of Na^+ in the SSM bathing solution only a small artifact was obtained, the same experiment at pH 4.7 produced signals also in the absence of Na^+. Note that the measurements of Figure 6D were recorded using the same sample which allows direct comparison of the current amplitudes at pH 4.7 and 7.4.

To confirm that the observed electrical signal is due to the transport activity of $GltP_{Ph}$, we tested specific inhibitors of glutamate transport. A 1 mM L-glutamate concentration

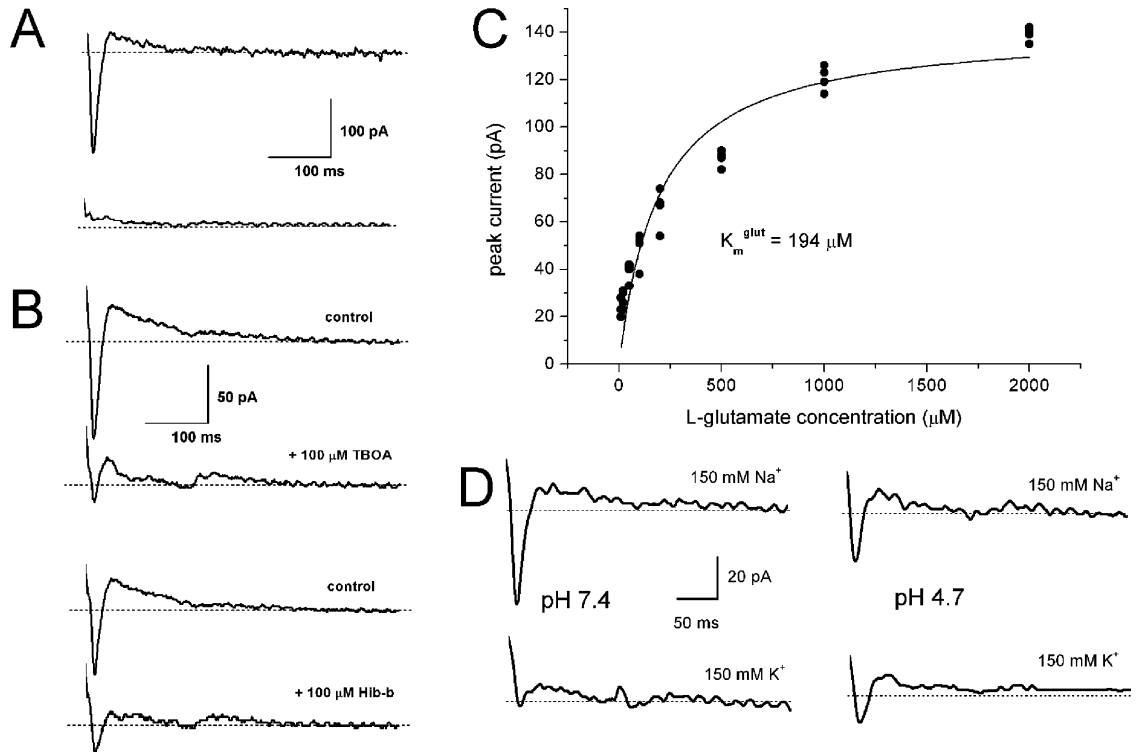

FIGURE 6: (A) Electrical signals generated by $GltP_{Ph}$ after different solution exchange protocols. In addition to the salts given below, resting, activating, and nonactivating solutions contained 30 mM HEPES (pH 7.4), 2 mM $MgCl_2$, 0.3 mM $CaCl_2$, and 0.1 mM dithiothreitol. All the data shown in the figure were recorded on the same sample. At the beginning of the trace, the nonactivating solution was replaced with the activating solution. The top trace is for the resting solution which contains 150 mM KCl, the nonactivating solution which contains 150 mM NaCl, and the activating solution which contains 150 mM NaCl, and 2 mM Tris-L-glutamate. The bottom trace is for the resting solution which contains 150 mM KCl, the nonactivating solution which contains 150 mM KCl, and the activating solution which contains 150 mM KCl and 2 mM Tris-L-glutamate. (B) Inhibition of the transient electrical signal by TBOA and HIP-B. In addition to the inhibitor and the salts given below, resting, activating, and nonactivating solutions contained 30 mM HEPES (pH 7.4), 2 mM $MgCl_2$, 0.3 mM $CaCl_2$, and 0.1 mM dithiothreitol. The resting solution contained 150 mM KCl, the nonactivating solution 150 mM NaCl, and the activating solution 150 mM NaCl and 1 mM Tris-L-glutamate. The top trace is the corresponding control signal recorded after washing out the inhibitor. (C) L-Glutamate concentration dependence of the peak current of the transient electrical signal after a glutamate concentration jump. Conditions: resting solution which contains 150 mM KCl, nonactivating solution which contains 150 mM NaCl, and activating solution which contains 150 mM NaCl and Tris-L-glutamate as indicated in the figure. The solid line is a fit to the data with a hyperbolic function. (D) Comparison of the transient electrical signal at pH 7.4 and 4.7. In addition to the salts given below, resting, activating, and nonactivating solutions contained 30 mM HEPES (pH 7.4) or 30 mM acetate (pH 4.7), 2 mM $MgCl_2$, 0.3 mM $CaCl_2$, and 0.1 mM dithiothreitol. The top traces (150 mM Na^+) are for the resting solution which contains 150 mM KCl, the nonactivating solution which contains 150 mM NaCl, and the activating solution which contains 150 mM NaCl and 1 mM Tris-L-glutamate. The bottom traces (150 mM K^+) are for the resting solution which contains 150 mM KCl, the nonactivating solution which contains 150 mM KCl, and the activating solution which contains 150 mM KCl and 1 mM Tris-L-glutamate.

jump was performed in the absence (top trace) and presence (bottom trace) of the inhibitors (Figure 6B). Indeed, a significant reversible reduction of the glutamate-induced current was observed with 100 μM TBOA (threo-β-benzyloxyaspartic acid) and HIP-B (3-hydroxy-4,5,6,6a-tetrahydro-3a*H*-pyrolo[3,4-*d*]isoxazole-6-carboxylic acid), two inhibitors of eukaryotic Na^+-dependent excitatory amino acid transporters (*42*, *43*).

Glutamate Concentration Dependence of $GltP_{Ph}$ Glutamate Transport. To determine the half-saturation concentration for $GltP_{Ph}$ glutamate transport activation ($K_{0.5}^{glut}$), we imposed L-glutamate concentration jumps of varying amplitudes and recorded the peak currents (I_p) (Figure 6C). Four different measurements were normalized to the average values obtained at glutamate concentrations between 10 μM and 2 mM and averaged. The signal amplitude increased with an increasing glutamate concentration. A fit with the hyperbolic function $I_p = I_p^{max}c/(c + K_{0.5}^{glut})$ (c is the L-glutamate concentration) yielded a half-saturation concentration ($K_{0.5}^{glut}$) of 194 μM.

DISCUSSION

We used different methods to determine the oligomeric state of prokaryotic glutamate transporters $GltP_{Ec}$ and $GltP_{Ph}$ in detergent solution and in the membrane.

Single-particle analysis indicated that $GltP_{Ph}$ is a stable trimer in detergent solution, consistent with other biochemical results (*18*, *20*). $GltP_{Ph}$ is trimeric in three-dimensional (3D) crystals (*17*). The negatively stained single particles showed a large ~45 Å stain-filled central cavity. This corresponds most likely to the 50 Å wide and 30 Å deep basin observed in the X-ray structure (*17*). As the individual monomers in a glutamate transporter trimer function independently (*44*), this basin, which allows the aqueous solution to reach the midpoint of the membrane bilayer, is the most likely explanation for a trimerization of the transporter. In addition, a trimer may be more stable in the membrane than monomers.

We used 2D crystallization to show the transporter's low-resolution projection structure and its oligomeric state in the membrane. 2D crystallization has an advantage over 3D

crystallization in that the detergent-solubilized membrane protein is reconstituted in a lipid bilayer, which is very similar to its native environment. We obtained 2D crystals of $GltP_{Ph}$ with a 3-fold symmetry that showed unambiguously that the transporter also forms stable trimers in the membrane. The dimensions of the $GltP_{Ph}$ monomer in 2D crystals (31 Å × 46 Å) were very similar to those in 3D crystals (*17*). As with the single particles, we also observed a 45 Å cavity formed by the trimeric assembly of monomers.

$GltP_{Ph}$ eluted from a calibrated Superose-6 column as a single peak like its homologue $GltP_{Ec}$, which exhibited besides the main peak an additional higher-molecular mass shoulder. Judging from the molecular masses of the soluble protein standards, and without considering different protein shapes and different amounts of detergent or lipid bound to the proteins, the peaks would correspond to a molecular mass of ~360 kDa for $GltP_{Ph}$ and ~380 and ~620 kDa for $GltP_{Ec}$. Because of the unknown amount of bound detergent or lipid, gel filtration is not a suitable method for determining accurately the oligomeric state of a membrane protein. However, since $GltP_{Ph}$ was shown to be a trimer in detergent solution and since both homologous transporters eluted at the same point, it is likely that the $GltP_{Ec}$ peak also corresponds to a trimer. That the $GltP_{Ec}$ trimer is the most abundant oligomeric form in detergent solution was also supported by our blue-native gel electrophoresis results and cross-linking with glutaraldehyde.

Furthermore, the results of the blue-native gel electrophoresis as well as cross-linking with DSS proved the existence of a $GltP_{Ec}$ hexamer as the only higher oligomer in detergent solution. The second oligomeric $GltP_{Ec}$ form, appearing as a shoulder at a higher molecular mass in gel filtration, corresponds therefore most likely to a hexamer. The observed reversible trimer−hexamer equilibrium depended on the protein concentration and on the type of detergent used. These results are consistent with data obtained with eukaryotic glutamate transporter GLT-1 (*19*) and are comparable with reports on the solubilized protein translocation complex SecYEG, where a detergent-mediated change in the oligomeric state was found (*45*).

$GltP_{Ph}$ is a trimer in the membrane and in detergent solution. Since $GltP_{Ph}$ as a protein from a thermophilic organism is more stable in solution than its *E. coli* homologue, the observed $GltP_{Ec}$ hexamer might be due to aggregation caused by the detergent. However, if this were the case, we would expect a ladderlike pattern of aggregates of increasing size on the blue-native gels. Moreover, since we observed a reversible equilibrium between the trimer and hexamer, we can exclude the possibility that the hexamer represents just the first step in nonspecific aggregation. The trimer−hexamer equilibrium of $GltP_{Ec}$ might also be a reason the protein did not crystallize.

Both transporters were fully active upon reconstitution into liposomes, as shown by uptake of radioactively labeled L-aspartate or L-glutamate. Glutamate transport by $GltP_{Ec}$ depended on only a proton gradient. This is consistent with transport studies on *E. coli* membrane vesicles (*16*) but in contrast to studies by Gendreau et al., who assessed a Na^+-dependent glutamate uptake of purified and reconstituted $GltP_{Ec}$ (*20*).

$GltP_{Ph}$-catalyzed glutamate transport required cotransport of protons or Na^+. A Na^+−H^+−L-glutamate symport has also been found for the glutamate transporters from *B. stearothermophilus* and *B. caldotenax* (*16*). However, these transporters lost their coupling Na^+ selectivity when they were expressed in *E. coli*, and glutamate transport was no longer stimulated by a Na^+ cotransport. By comparison, glutamate transport in eukaryotes is more complex; e.g., GLT-1-catalyzed glutamate transport involves cotransport of three sodium ions, a proton, and one glutamate in exchange for a potassium ion (*7*, *8*).

Adsorption of proteoliposomes to a solid-supported membrane (SSM) allows the investigation of charge transport in proteins that are not amenable to conventional electrophysiology, such as bacterial transporters. This technique is particularly suited to monitoring rapid pre-steady-state charge displacements while stationary transport activity is difficult to assess (*25*). It is, therefore, an excellent complement to the transport measurements described above. A fast transient current corresponding to the translocation of negative charge into $GltP_{Ph}$ proteoliposomes coupled to the SSM was observed after a L-glutamate concentration jump. This signal was strictly dependent on the presence of Na^+ outside but did not require an inward-directed Na^+ gradient or any K^+ inside the liposomes. This is consistent with our observations on the melibiose transporter and other transport proteins (*46*) which also do not require an ion gradient in pre-steady-state experiments. Na^+ can be replaced with H^+ as demonstrated by experiments at acidic pH 4.7 in the absence of Na^+, a result which is in agreement with the uptake studies presented above. In addition, the L-glutamate-induced charge translocation could be inhibited by specific inhibitors of glutamate transporters TBOA and HIP-B. There is, therefore, no doubt that the electrical signal is correlated to the transport activity of $GltP_{Ph}$.

The affinity of the transporter for L-glutamate of ~200 μM, as determined from the transient currents, is considerably lower than the literature values for other glutamate transporters of only a few micromolar (*16*). One reason may be that our value corresponds to the cytoplasmic glutamate binding site (note that we have no information about the orientation of $GltP_{PH}$ in the liposomal membrane). Also, the fact that our data are pre-steady-state data rather than steady-state data may be important. In pre-steady-state data, the early steps rather than the rate-limiting reaction determine the kinetics. This may yield apparent affinities different from those of steady-state data. Another reason for the observed low affinity may be the difference between the operation temperature of $GltP_{Ph}$ in vivo (~95 °C) and the temperature at which the experiments were carried out (~22 °C).

The electrical signals indicate that during or immediately following glutamate binding negative charge is displaced into the liposomes in a rapid process exceeding the time resolution of the technique (~15 ms). This is followed by a slower reaction (~70 ms) displacing positive charge into the liposome. A tentative explanation for the biphasic signal could be the translocation of the glutamate anion (fast negative transient of the electrical signal; $\tau \sim 8$ ms) followed by the uptake of Na^+ (positive phase; $\tau \sim 70$ ms). Alternatively, substrate binding and/or transport could induce an electrogenic conformational transition in the protein displacing negative and/or positive charge. Electrogenic conformational transitions have indeed been found in Na^+-coupled cotransporters (*46*), and conformational transitions

upon substrate binding have been demonstrated in glutamate transporters (*47*).

In summary, our results show that $GltP_{Ph}$ is indeed a glutamate transporter that is more similar in its transport mechanism to its eukaryotic homologues than $GltP_{Ec}$.

ACKNOWLEDGMENT

We thank Lina Hatahet for excellent technical assistance, Deryck Mills and Janet Vonck for help with electron microscopy and data processing, David Parcej for helpful discussions, Winfried Haase for freeze-fracture analysis of proteoliposomes, and Mihnea Bostina for help with the single-particle analysis.

REFERENCES

1. Headley, P. M., and Grillner, S. (1990) Excitatory amino acids and synaptic transmission: The evidence for a physiological function, *Trends Pharmacol. Sci. 11*, 205−211.
2. Storck, T., Schulte, S., Hofmann, K., and Stoffel, W. (1992) Structure, expression, and functional analysis of a Na^+-dependent glutamate/aspartate transporter from rat brain, *Proc. Natl. Acad. Sci. U.S.A. 89*, 10955−10959.
3. Pines, G., Danbolt, N. C., Bjoras, M., Zhang, Y., Bendahan, A., Eide, L., Koepsell, H., Storm-Mathisen, J., Seeberg, E., and Kanner, B. I. (1992) Cloning and expression of a rat brain L-glutamate transporter, *Nature 360*, 464−467 [comment erratum, (1992) *Nature 360* (6406), 768; comment, (1992) *Nature 360* (6403), 420−421].
4. Kanai, Y., and Hediger, M. A. (1992) Primary structure and functional characterization of a high-affinity glutamate transporter, *Nature 360*, 467−471.
5. Fairman, W. A., Vandenberg, R. J., Arriza, J. L., Kavanaugh, M. P., and Amara, S. G. (1995) An excitatory amino-acid transporter with properties of a ligand-gated chloride channel, *Nature 375*, 599−603.
6. Arriza, J. L., Eliasof, S., Kavanaugh, M. P., and Amara, S. G. (1997) Excitatory amino acid transporter 5, a retinal glutamate transporter coupled to a chloride conductance, *Proc. Natl. Acad. Sci. U.S.A. 94*, 4155−4160.
7. Kanner, B. I., and Bendahan, A. (1982) Binding order of substrates to the sodium and potassium ion coupled L-glutamic acid transporter from rat brain, *Biochemistry 21*, 6327−6330.
8. Pines, G., and Kanner, B. I. (1990) Counterflow of L-glutamate in plasma membrane vesicles and reconstituted preparations from rat brain, *Biochemistry 29*, 11209−11214.
9. Kavanaugh, M. P., Bendahan, A., Zerangue, N., Zhang, Y., and Kanner, B. I. (1997) Mutation of an amino acid residue influencing potassium coupling in the glutamate transporter GLT-1 induces obligate exchange, *J. Biol. Chem. 272*, 1703−1708.
10. Halpern, Y. S. M. L. (1965) Glutamate transport in wild-type and mutant strains of *Escherichia coli*, *J. Bacteriol. 90*, 1288−1295.
11. Casadaban, M. J., Chou, J., and Cohen, S. N. (1980) In vitro gene fusions that join an enzymatically active β-galactosidase segment to amino-terminal fragments of exogenous proteins: *Escherichia coli* plasmid vectors for the detection and cloning of translational initiation signals, *J. Bacteriol. 143*, 971−980.
12. Halpern, Y. S., Barash, H., Dover, S., and Druck, K. (1973) Sodium and potassium requirements for active transport of glutamate by *Escherichia coli* K-12, *J. Bacteriol. 114*, 53−58.
13. Halpern, Y. S., Barash, H., and Druck, K. (1973) Glutamate transport in *Escherichia coli* K-12: Nonidentity of carriers mediating entry and exit, *J. Bacteriol. 113*, 51−57.
14. Miner, K. M., and Frank, L. (1974) Sodium-stimulated glutamate transport in osmotically shocked cells and membrane vesicles of *Escherichia coli*, *J. Bacteriol. 117*, 1093−1098.
15. Schellenberg, G. D., and Furlong, C. E. (1977) Resolution of the multiplicity of the glutamate and aspartate transport systems of *Escherichia coli*, *J. Biol. Chem. 252*, 9055−9064.
16. Tolner, B., Ubbink-Kok, T., Poolman, B., and Konings, W. N. (1995) Cation-selectivity of the L-glutamate transporters of *Escherichia coli*, *Bacillus stearothermophilus*, and *Bacillus caldotenax*: Dependence on the environment in which the proteins are expressed, *Mol. Microbiol. 18*, 123−133.
17. Yernool, D., Boudker, O., Jin, Y., and Gouaux, E. (2004) Structure of a glutamate transporter homologue from *Pyrococcus horikoshii*, *Nature 431*, 811−818.
18. Yernool, D., Boudker, O., Folta-Stogniew, E., and Gouaux, E. (2003) Trimeric subunit stoichiometry of the glutamate transporters from *Bacillus caldotenax* and *Bacillus stearothermophilus*, *Biochemistry 42*, 12981−12988.
19. Raunser, S., Haase, W., Bostina, M., Parcej, D. N., and Kuhlbrandt, W. (2005) High-yield expression, reconstitution and structure of the recombinant, fully functional glutamate transporter GLT-1 from *Rattus norvegicus*, *J. Mol. Biol. 351*, 598−613.
20. Gendreau, S., Voswinkel, S., Torres-Salazar, D., Lang, N., Heidtmann, H., Detro-Dassen, S., Schmalzing, G., Hidalgo, P., and Fahlke, C. (2004) A trimeric quaternary structure is conserved in bacterial and human glutamate transporters, *J. Biol. Chem. 279*, 39505−39512.
21. Tolner, B., Poolman, B., Wallace, B., and Konings, W. N. (1992) Revised nucleotide sequence of the gltP gene, which encodes the proton-glutamate-aspartate transport protein of *Escherichia coli* K-12, *J. Bacteriol. 174*, 2391−2393.
22. Deguchi, Y., Yamato, I., and Anraku, Y. (1989) Molecular cloning of gltS and gltP, which encode glutamate carriers of *Escherichia coli* B, *J. Bacteriol. 171*, 1314−1319.
23. Sambrook, J., Fritsch, E. F., and Maniatis, T. (1989) *Molecular Cloning, A laboratory manual*, 2nd ed., Cold Spring Harbor Laboratory Press, Plainview, NY.
24. Pintschovius, J., and Fendler, K. (1999) Charge translocation by the Na^+/K^+-ATPase investigated on solid supported membranes: Rapid solution exchange with a new technique, *Biophys. J. 76*, 814−826.
25. Ganea, C., Pourcher, T., Leblanc, G., and Fendler, K. (2001) Evidence for intraprotein charge transfer during the transport activity of the melibiose permease from *Escherichia coli*, *Biochemistry 40*, 13744−13752.
26. Bamberg, E., Alpes, H., Apell, H. J., Bradley, R., Harter, B., Quelle, M. J., and Urry, D. W. (1979) Formation of ionic channels in black lipid membranes by succinic derivatives of gramicidin A, *J. Membr. Biol. 50*, 257−270.
27. Bradford, M. M. (1976) A rapid and sensitive method for the quantitation of microgram quantities of protein utilizing the principle of protein-dye binding, *Anal. Biochem. 72*, 248−254.
28. Schagger, H., Cramer, W. A., and von Jagow, G. (1994) Analysis of molecular masses and oligomeric states of protein complexes by blue native electrophoresis and isolation of membrane protein complexes by two-dimensional native electrophoresis, *Anal. Biochem. 217*, 220−230.
29. Schagger, H., and von Jagow, G. (1991) Blue native electrophoresis for isolation of membrane protein complexes in enzymatically active form, *Anal. Biochem. 199*, 223−231.
30. Frank, J., Radermacher, M., Penczek, P., Zhu, J., Li, Y., Ladjadj, M., and Leith, A. (1996) SPIDER and WEB: Processing and visualization of images in 3D electron microscopy and related fields, *J. Struct. Biol. 116*, 190−199.
31. Radermacher, M., Wagenknecht, T., Verschoor, A., and Frank, J. (1987) Three-dimensional reconstruction from a single-exposure, random conical tilt series applied to the 50S ribosomal subunit of *Escherichia coli*, *J. Microsc. 146* (Part 2), 113−136.
32. Marco, S., Chagoyen, M., de la Fraga, L. G., and Carazo, J. M. (1996) A variant to the radon approximation of the reference-free alignment algorithm, *Ultramicroscopy 66*, 5−10.
33. Radermacher, M. (1997) Radon Transform Techniques for Alignment and Three-dimensional Reconstruction from Random Projections, *Scanning Microsc. 11*, 171−177.
34. Radermacher, M., Ruiz, T., Wieczorek, H., and Gruber, G. (2001) The structure of the V_1-ATPase determined by three-dimensional electron microscopy of single particles, *J. Struct. Biol. 135*, 26−37.
35. Marabini, R., and Carazo, J. M. (1994) Pattern recognition and classification of images of biological macromolecules using artificial neural networks, *Biophys. J. 66*, 1804−1814.
36. Marabini, R., Masegosa, I. M., San Martin, M. C., Marco, S., Fernandez, J. J., de la Fraga, L. G., Vaquerizo, C., and Carazo, J. M. (1996) Xmipp: An Image Processing Package for Electron Microscopy, *J. Struct. Biol. 116*, 237−240.
37. Crowther, R. A., Henderson, R., and Smith, J. M. (1996) MRC image processing programs, *J. Struct. Biol. 116*, 9−16.
38. Henderson, R., Jubb, J. S., and Rossmann, M. G. (1982) A contracted form of the trigonal purple membrane of *Halobacterium halobium*, *J. Mol. Biol. 154*, 501−514.

39. Vinothkumar, K. R., Raunser, S., Jung, H., and Kuhlbrandt, W. (2006) Oligomeric structure of the carnitine transporter CaiT from *Escherichia coli*, *J. Biol. Chem. 281*, 4795−4801.
40. Heuberger, E. H., Veenhoff, L. M., Duurkens, R. H., Friesen, R. H., and Poolman, B. (2002) Oligomeric state of membrane transport proteins analyzed with blue native electrophoresis and analytical ultracentrifugation, *J. Mol. Biol. 317*, 591−600.
41. Valpuesta, J. M., Carrascosa, J. L., and Henderson, R. (1994) Analysis of electron microscope images and electron diffraction patterns of thin crystals of ϕ29 connectors in ice, *J. Mol. Biol. 240*, 281−287.
42. Shimamoto, K., Lebrun, B., Yasuda-Kamatani, Y., Sakaitani, M., Shigeri, Y., Yumoto, N., and Nakajima, T. (1998) DL-*threo*-β-Benzyloxyaspartate, a potent blocker of excitatory amino acid transporters, *Mol. Pharmacol. 53*, 195−201.
43. Funicello, M., Conti, P., De Amici, M., De Micheli, C., Mennini, T., and Gobbi, M. (2004) Dissociation of [^{3}H]L-glutamate uptake from L-glutamate-induced [^{3}H]D-aspartate release by 3-hydroxy-4,5,6,6a-tetrahydro-3a*H*-pyrrolo[3,4-*d*]isoxazole-4-carboxylic acid and 3-hydroxy-4,5,6,6a-tetrahydro-3a*H*-pyrrolo[3,4-*d*]isoxazole-6-carboxylic acid, two conformationally constrained aspartate and glutamate analogs, *Mol. Pharmacol. 66*, 522−529.
44. Grewer, C., Balani, P., Weidenfeller, C., Bartusel, T., Tao, Z., and Rauen, T. (2005) Individual subunits of the glutamate transporter EAAC1 homotrimer function independently of each other, *Biochemistry 44*, 11913−11923.
45. Bessonneau, P., Besson, V., Collinson, I., and Duong, F. (2002) The SecYEG preprotein translocation channel is a conformationally dynamic and dimeric structure, *EMBO J. 21*, 995−1003.
46. Meyer-Lipp, K., Ganea, C., Pourcher, T., Leblanc, G., and Fendler, K. (2004) Sugar binding induced charge translocation in the melibiose permease from *Escherichia coli*, *Biochemistry 43*, 12606−12613.
47. Larsson, H. P., Tzingounis, A. V., Koch, H. P., and Kavanaugh, M. P. (2004) Fluorometric measurements of conformational changes in glutamate transporters, *Proc. Natl. Acad. Sci. U.S.A. 101*, 3951−3956.

BI061008+